

Fig. 2. Expression level of G_{α12} proteins in the heart. *A*: representative Western blots of G_{α12} proteins and tubulin. Whole cell fractions of hearts were subjected to SDS-PAGE and immunoblot analysis. *B*: pooled data of the expression level of G_{α12} proteins normalized to that of tubulin. Graph shows means ± SE; *n* = 5.

of control myocytes; therefore, GPCR-mediated activation of G_{i/o} induced abnormal SS and TT LTCC current densities in ISO myocytes.

Effect of the LTCC agonist Bay K8644 on LTCC density. Next, we examined whether the observed differences in SS and TT LTCC current density among the four groups of myocytes could be ascribed to alteration in the gating and/or expression levels of LTCCs. The density of macroscopic LTCC currents (*D*) can be described by the following equation: $D = N \times A \times P_o \times i/C_m$, where *N* is the number of channels, *A* is the availability, *P_o* is the open probability, *i* is the single channel current amplitude, and *C_m* is the membrane capacitance. The LTCC agonist Bay K8644 (1 μmol/l) almost maximally increases $A \times P_o$ but does not affect other parameters by selectively modulating the gating of LTCCs (18). Figure 4*A* shows SS and TT LTCC current densities in the presence of Bay K8644 (1 μmol/l). Surprisingly, Bay K8644 almost completely abolished the difference in LTCC current density among whole cell, SS, and TT membranes and among the four groups of myocytes. Thus, the observed differences in LTCC density (Fig. 3*C*) seem to be ascribed to a difference in the gating but not the expression level of LTCCs. We also calculated the ratio of LTCC current density in the absence of Bay K8644 to that in the presence of the drug, a parameter reflecting $A \times P_o$ (Fig. 4*B*). The profile of the plot of this parameter closely resembled that of LTCC current density (Fig. 3*C*). Therefore, it is likely that in heart failure, GPCR-mediated activation of G_{i/o} decreased TT LTCC current density and increased SS LTCC current density in ISO myocytes by decreasing or increasing *A* and/or *P_o* of LTCCs, respectively.

Effect of a selective PKA inhibitor on the modulation of LTCC current density by PTX. G_{i/o} inhibits adenylyl cyclase (32). Thus, PTX might have increased intracellular cAMP concentration and PKA activity and thereby normalized the TT LTCC activity in ISO + PTX myocytes (27). We thus examined the effect of a selective PKA inhibitor, H-89 (1 μM), on

LTCC activity. H-89 did not significantly affect LTCC current densities in control or ISO myocytes, as previously reported (Fig. 5) (19). This indicates that PKA was not activated in these myocytes and that the increased SS LTCC current density in ISO myocytes was not due to the effect of ISO possibly remaining in the preparation of isolated myocytes. H-89 also did not affect LTCC current densities in PTX myocytes, indicating that PTX on its own did not significantly activate PKA. Finally, H-89 did not decrease TT LTCC current density or increase SS LTCC current density in ISO + PTX myocytes. We found that H-89 (10 μmol/l) also did not affect SS or TT LTCC current density in any of the four groups of myocytes

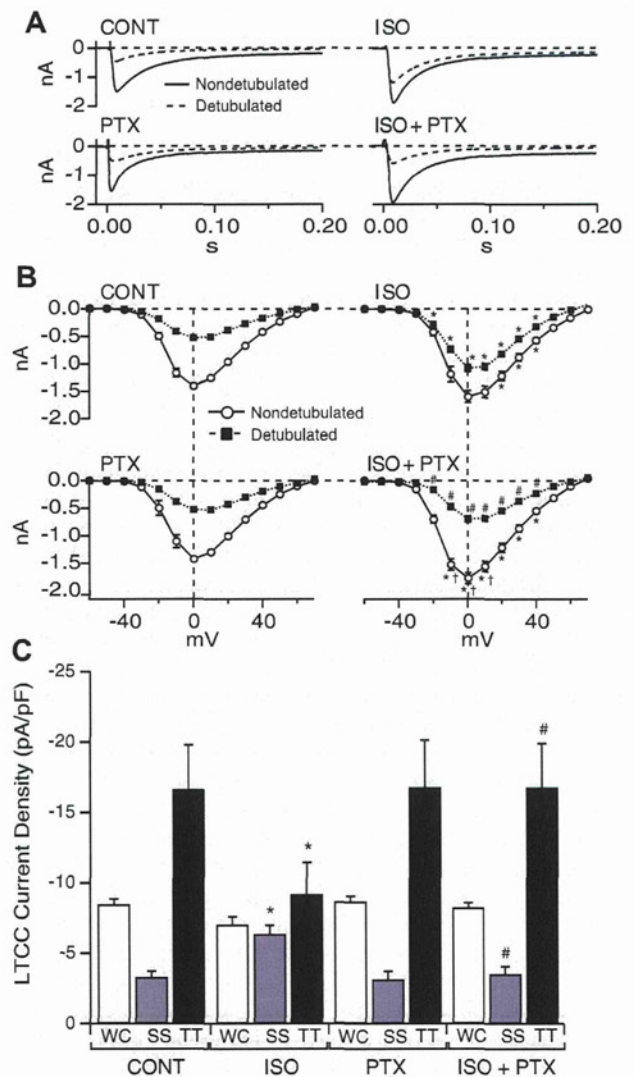


Fig. 3. Effect of PTX on L-type Ca²⁺ channel (LTCC) current densities in whole cell (WC), surface sarcolemmal (SS), and t-tubular (TT) membranes. *A*: representative LTCC currents at 0 mV in control, ISO, PTX, and ISO + PTX myocytes with and without detubulation. *B*: peak current-voltage relationships of LTCC currents in control, ISO, PTX, and ISO + PTX myocytes with and without detubulation. *C*: LTCC current density at 0 mV in WC, SS, and TT membranes in control, ISO, PTX, and ISO + PTX myocytes. Graphs show means ± SE; *n* = 6–8 for each group. **P* < 0.05 vs. control; #*P* < 0.05 vs. ISO; †*P* < 0.05 vs. PTX.

Table 2. Parameters used for the fitting of relationship between whole cell LTCC current density and membrane potential and inactivation of whole cell LTCC currents at different membrane potentials

| | Control | ISO | PTX | ISO + PTX |
|--|---------------|---------------|---------------|---------------|
| Activation | | | | |
| G_{max} , pS/pF | 128.90 ± 5.62 | 114.97 ± 8.96 | 135.50 ± 5.00 | 130.75 ± 6.14 |
| $E_{0.5_Act}$, mV | -14.78 ± 0.64 | -12.31 ± 1.46 | -13.80 ± 1.76 | -15.43 ± 0.80 |
| k_{Act} , mV | 4.79 ± 0.09 | 4.77 ± 0.23 | 4.84 ± 0.09 | 4.88 ± 0.06 |
| E_{rev} , mV | 63.76 ± 1.15 | 66.32 ± 0.98 | 64.12 ± 1.40 | 63.00 ± 0.70 |
| Inactivation (R_{100}) | | | | |
| -20 mV | 0.45 ± 0.02 | 0.47 ± 0.04 | 0.41 ± 0.07 | 0.41 ± 0.04 |
| 0 mV | 0.17 ± 0.01 | 0.19 ± 0.01 | 0.15 ± 0.00 | 0.17 ± 0.01 |
| +20 mV | 0.26 ± 0.02 | 0.28 ± 0.02 | 0.22 ± 0.03 | 0.26 ± 0.01 |
| +40 mV | 0.39 ± 0.03 | 0.38 ± 0.03 | 0.33 ± 0.06 | 0.38 ± 0.04 |

Values are means ± SE; $n = 8$ for the control group, 6 for the ISO group, 6 for the PTX group, and 8 for the ISO + PTX group. G_{max} , maximum conductance density; $E_{0.5_Act}$, half-maximum activation potential; k_{Act} , slope factor of activation; E_{rev} , apparent reversal potential of L-type Ca²⁺ channel (LTCC) currents; R_{100} , fraction of LTCC currents remaining 100 ms after depolarization.

(data not shown); therefore, the cAMP/PKA pathway did not mediate the effect of PTX.

Effect of a selective PP2A inhibitor on the modulation of LTCC current density by PTX. We (19) previously found that an inhibitor of PP1 and PP2A (OA) did not increase TT LTCC current density in control myocytes but normalized the decreased TT LTCC density in ISO myocytes, indicating that the activation of PP1/2A caused a decrease in TT LTCC current density in ISO myocytes (19). On the other hand, OA increased SS LTCC current density in control myocytes but did not further enhance increased SS LTCC current density in ISO myocytes, indicating that the suppression of PP1/2A resulted in increased SS LTCC current density in ISO myocytes. Thus, we first examined the expression levels of PP1 and PP2A in the four groups of hearts (Fig. 6). There were no significant differences in the expression levels of PP1 or PP2A among the four groups of mice. We next examined the effect of a selective PP2A inhibitor, fostriecin (1 μM), on LTCC activity. Fostriecin did not significantly change LTCC current densities in control myocytes (Fig. 7A). This result and the above result with OA indicate that SS LTCC activity was suppressed by PP1 in control myocytes and that this suppression was lost in ISO myocytes. Fostriecin did not significantly change SS LTCC current density but almost completely normalized TT LTCC current density in ISO myocytes. Thus, PP2A suppressed TT LTCC activity in ISO myocytes. Fostriecin did not affect LTCC current densities in PTX myocytes. Fostriecin also did not increase SS LTCC current density in ISO + PTX myocytes, indicating that PTX suppressed SS LTCC activity by activating PP1 in ISO + PTX myocytes. On the other hand, fostriecin did not further enhance the increased TT LTCC current density in ISO + PTX myocytes. Thus, the effect of fostriecin on TT LTCC activity was occluded and therefore PTX enhanced TT LTCC activity by inhibiting PP2A in ISO + PTX myocytes. We further found that OA occluded the effect of fostriecin on TT LTCC activity in ISO myocytes and vice versa (Fig. 7B), indicating that OA and fostriecin caused their effect on the TT LTCC activity by inhibiting a common target, PP2A. Therefore, GPCR-mediated activation of G_{i/o} decreased basal TT LTCC activity by activating PP2A, whereas it increased basal SS LTCC activity by inhibiting PP1 in ISO myocytes.

DISCUSSION

In the present study, we examined whether activation of G_{i/o} was responsible for the abnormal E-C coupling in ISO mice by chronically administering PTX to ISO mice. ISO + PTX mice exhibited significantly higher FS (Fig. 1D) and higher TT LTCC current density and lower SS LTCC current density (Fig. 3C) than ISO mice. These changes in LTCC density were likely to have resulted from alterations in the gating but not expression levels of LTCCs (Fig. 4B). PTX normalized basal TT LTCC activity by inhibiting PP2A and basal SS LTCC activity by activating PP1 independently of PKA (Figs. 5 and 7).

Role of G_{i/o} in cardiac hypertrophy and failure. As ISO mice, ISO + PTX mice showed significant cardiac hypertrophy compared with control or PTX mice (Fig. 1, A and B), indicating that ISO caused cardiac hypertrophy via G_s. On the other hand, ISO + PTX mice showed significantly higher FS than ISO mice (Fig. 1D). Thus, GPCR-mediated activation of G_{i/o} at least partially accounted for the impaired cardiac function of ISO mice.

In the heart, activation of G_i attenuates ISO-stimulated but not basal ventricular contractility in an acute setting (accentuated antagonism) (9). Although several mechanisms have been proposed to underlie this phenomenon, the most important is the direct inhibition of adenylyl cyclase by G_i. Thus, the effect of PTX on cardiac contractility found in ISO + PTX mice may have resulted from removal of the inhibitory effect of G_i on adenylyl cyclase activated by ISO or endogenous catecholamines. However, the effect of PTX on cardiac contractility may not be explained only in terms of the suppression of the accentuated antagonism if the effect of PTX on LTCCs in isolated ISO myocytes is taken into account.

In isolated myocytes, PTX normalized the abnormalities in the LTCC activity found in ISO myocytes (Fig. 3C). In addition, H-89 did not affect SS or TT LTCC activity in ISO or ISO + PTX myocytes (Fig. 5) (19). Therefore, it is likely that GPCR-mediated activation of G_{i/o} modulated basal SS and TT LTCC activity independently of PKA in heart failure. Because this effect of G_{i/o} is not observed with acute activation of G_{i/o}-coupled GPCRs in normal adult cardiac myocytes in vitro (27), it may be chronically built up in vivo in decompensated cardiac myocytes.

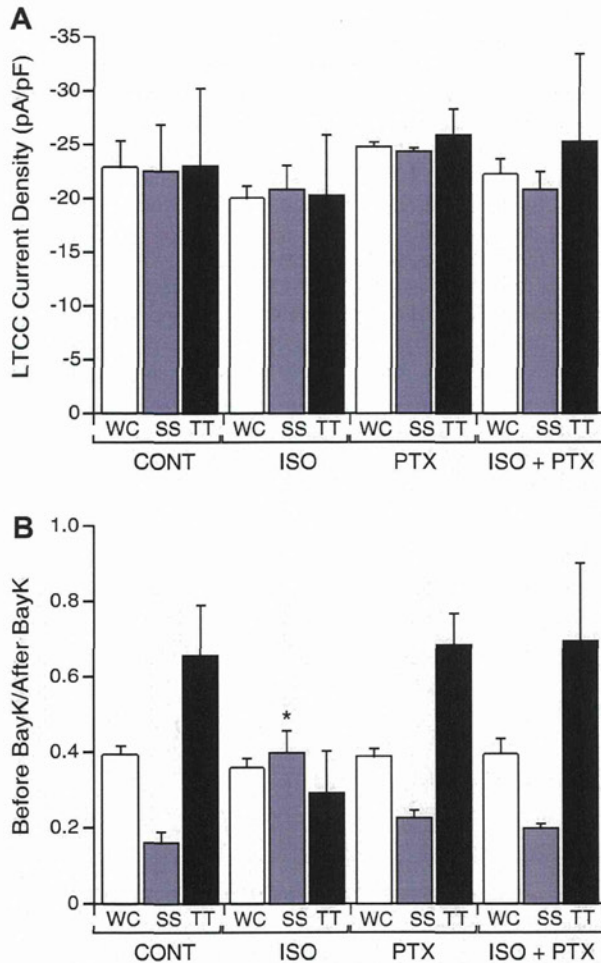


Fig. 4. Effect of Bay K8644 (BayK) on LTCC densities in WC, SS, and TT membranes. *A*: LTCC current density at 0 mV in WC, SS, and TT membranes in control, ISO, PTX, and ISO + PTX myocytes in the presence of BayK (1 μ mol/l). *B*: ratio of LTCC current density at 0 mV in the absence of BayK to that in the presence of BayK (1 μ mol/l) in WC, SS, and TT membranes in control, ISO, PTX, and ISO + PTX myocytes. Graphs show means \pm SE; $n = 6-8$ for each group. * $P < 0.05$ vs. control.

Role of PPs in heart failure. G_{i/o} inhibited TT LTCCs by activating PP2A, whereas it activated SS LTCCs by inhibiting PP1 in heart failure (Fig. 7A). Indeed, G_{i/o} is known to activate PP2A in cardiac myocytes (16, 22, 25). This reaction seems to be mediated by soluble guanylyl cyclase and p38 MAPK (25) and/or by small GTPase, Cdc42, and/or Rac1 and p21-activated kinase-1 (22). On the other hand, duBell and Rogers (8) recently reported that PP2A did not participate in the regulation of basal whole cell LTCC activity in normal mouse cardiac myocytes. We also found that fostriecin did not affect LTCC activity in control myocytes (Fig. 7A). Therefore, the suppression of basal TT LTCC activity by G_{i/o}-mediated activation of PP2A seems to be a de novo gain-of-function abnormality in heart failure. On the other hand, transgenic overexpression of constitutively active G_o suppressed PP1 and increased whole cell LTCC activity in cardiac myocytes (38). Because this reaction is also not observed with acute stimulation of G_{i/o}-coupled GPCRs in normal adult cardiac myocytes, G_o-medi-

ated suppression of the inhibitory effect of PP1 on SS LTCCs may also be newly established in heart failure.

It has often been reported that the expression level and/or activity of PP1/2A are increased in heart failure (4, 20, 28). Although we could not find the significantly increased expression of PPs in heart failure (Fig. 6), the present study indicates that PP2A activity is enhanced for TT LTCCs, whereas PP1 activity is suppressed for SS LTCCs, in heart failure. Such local regulation of LTCC activity may arise from colocalization of LTCCs and PPs and the resultant dephosphorylation of LTCCs in the microenvironment. Indeed, PP2A binds directly to the COOH-terminus of the Ca_v1.2 subunit of LTCCs (6, 15, 36), although a direct interaction between LTCCs and PP1 has not been reported to our knowledge. The molecular mechanism by which different types of PPs differentially interact with TT and SS LTCCs needs to be elucidated in future studies.

GPCRs activating G_{i/o} in heart failure. Because PTX normalized LTCC current densities in isolated myocytes (i.e., in the absence of GPCR agonists), the constitutive activity of GPCRs may activate G_{i/o}. In animal models of heart failure and patients with idiopathic dilated cardiomyopathy, the expression level of M₂-muscarinic acetylcholine and A₁ adenosine receptors is increased (12, 23, 33). Moreover, the phosphorylation of β_2 -ARs by PKA and GPCR kinase that expected to occur in heart failure switches their coupling from G_s to G_i (5, 26); therefore, these receptors may constitutively and chronically activate G_{i/o} and thereby cause abnormal LTCC activity in heart failure.

Functional significance of activation of G_{i/o} in heart failure. Many studies have demonstrated the dichotomous effects of increased G_{i/o} activity in heart failure: on one hand, it causes cardiac dysfunction by inhibiting cardiac contractility, whereas, on the other hand, it causes cardiac protection by preventing energy expenditure of the myocardium, pathological cardiac remodeling, myocyte apoptosis, and arrhythmias (9). Likewise, decreased TT LTCC activity must be deleterious for cardiac contractility, but this alteration may also be an adaptive mechanism to prevent early afterdepolarizations and fatal ventricular arrhythmias in heart failure (19, 37).

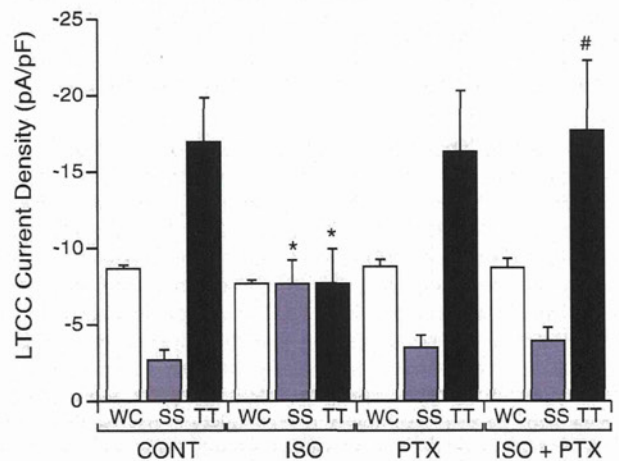


Fig. 5. Effect of a PKA inhibitor, H-89, on LTCC current densities in WC, SS, and TT membranes. LTCC current densities at 0 mV in WC, SS, and TT membranes in control, ISO, PTX, and ISO + PTX myocytes in the presence of H-89 (1 μ mol/l) are shown. Graph shows means \pm SE; $n = 6-7$ for each group. * $P < 0.05$ vs. control; # $P < 0.05$ vs. ISO.

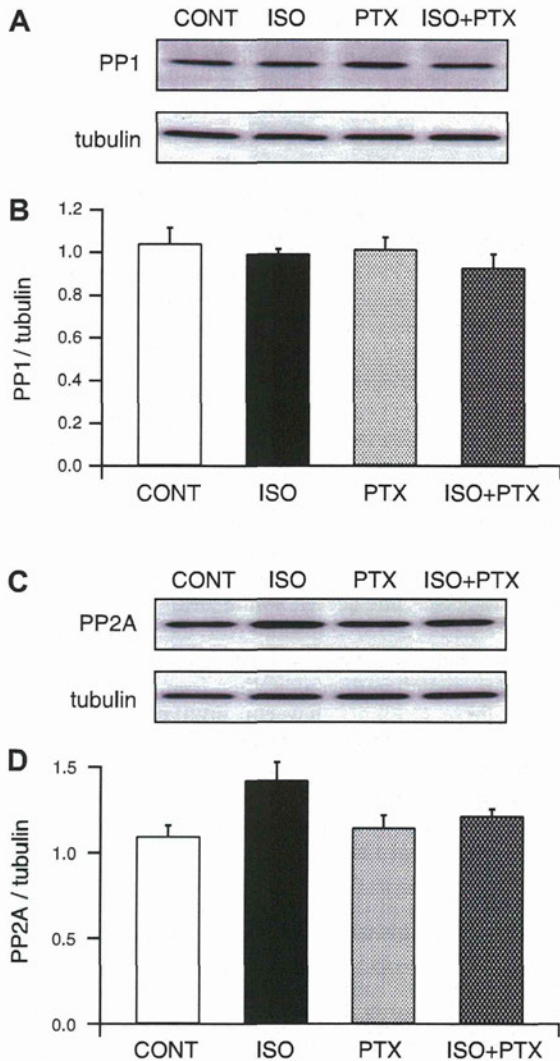


Fig. 6. Expression level of protein phosphatase (PP1) and PP2A in the heart. A: representative Western blots of PP1 and tubulin. B: pooled data of the expression level of PP1 normalized to that of tubulin. C: representative Western blots of PP2A and tubulin. D: pooled data of the expression level of PP2A normalized to that of tubulin. WC fractions of hearts were subjected to SDS-PAGE and immunoblot analysis. Graphs show means ± SE; n = 4.

Limitations. The systemic application of PTX must inactivate G_{i/o} not only in the heart but in other organs. Such extracardiac effects of PTX might indirectly ameliorate heart failure and normalize LTCC activity. For instance, PTX reduced blood pressure (24), which could improve cardiac function by reducing the afterload on the heart; however, we did not detect significant differences in MBP between ISO and ISO + PTX mice (Table 1), suggesting that this phenomenon is less likely to be involved in the amelioration of heart failure in ISO + PTX mice. PTX also increases HR (Table 1), sympathetic nerve activity (1), and renin release (14). These effects are expected to worsen rather than ameliorate heart failure and thus cannot account for the improvement of cardiac contractility of ISO + PTX mice. Nevertheless, it is necessary to confirm the present results with cardiac specific deletion of G_{i/o} genes in future studies.

It is also necessary to pay attention to the off-target effects of the pharmacological agents used in this study. H-89 has an IC₅₀ of 135 nM for PKA but also inhibits stress-activated protein kinase, p70 ribosomal protein S6 kinase, and Rho-dependent protein kinase with similar potency and efficacy as PKA (7); however, these kinases, other than PKA, are not known to modulate LTCCs. Fostriecin is ~40,000-fold more potent against PP2A (IC₅₀ = 3.2 nmol/l) than PP1 (IC₅₀ = 131 μmol/l) and virtually inactive against PP2B (34). Thus, 1 μmol/l fostriecin probably almost completely and selectively inhibited PP2A. The fact that OA and fostriecin mutually occluded the effect of one another on TT LTCC current density in ISO myocytes (Fig. 7B) underscores the specific action of fostriecin on PP2A. However, these results also need to be

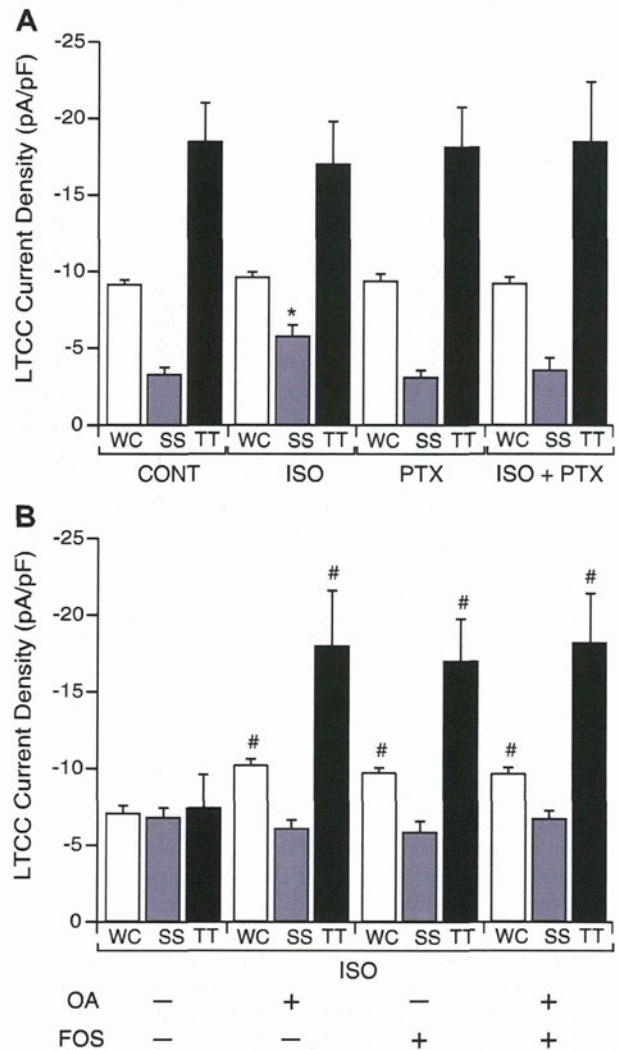


Fig. 7. Effect of a selective PP2A inhibitor, fostriecin (FOS), and a PP1 and PP2A inhibitor, okadaic acid (OA), on LTCC current densities in WC, SS, and TT membranes. A: LTCC current density at 0 mV in WC, SS, and TT membranes in control, ISO, PTX, and ISO + PTX myocytes in the presence of FOS (1 μmol/l). B: LTCC current density at 0 mV in WC, SS, and TT membranes in ISO myocytes in the presence of OA (1 μmol/l) and/or FOS (1 μmol/l). Graphs show means ± SE; n = 6–7 for each group. *P < 0.05 vs. control; #P < 0.05 vs. ISO.

confirmed with proteomic analysis of the phosphorylation status of LTCC in heart failure and deletion of PP genes in cardiac myocytes.

Concluding remarks. We showed that chronic GPCR-mediated activation of G_{i/o} decreases cardiac function at least partially by altering LTCC activity through PPs; however, a method to selectively inhibit G_{i/o}, such as PTX, is probably not adequate for the treatment of heart failure if the dichotomous effects of G_{i/o} in heart failure are taken into consideration. The present study rather supports the effectiveness of β -AR blocker therapy for heart failure, which not only increases the number of β -ARs but decreases the expression and activity of G_i in the failed myocardium (31). The present study also suggests that inverse agonists that suppress the constitutive activity of G_{i/o}-coupled GPCRs could be a useful adjunctive to β -AR blockers in heart failure therapy.

ACKNOWLEDGMENTS

The authors are grateful to Reiko Sakai for secretarial assistance.

GRANTS

This work was supported by Japan Society for the Promotion of Sciences Research Grant 21590275 (to M.Yamada) and Shinshu Public Utility Foundation for the Promotion of Medical Sciences Grants-In-Aid for Medical Scientific Research (to T. Kashiwara).

DISCLOSURES

No conflicts of interest, financial or otherwise, are declared by the author(s).

AUTHOR CONTRIBUTIONS

Author contributions: T.K., M. Hirose, and M.Y. conception and design of research; T.K., T.N., H.S., M.H.-H., S.G., and M. Hongo performed experiments; T.K., T.N., H.S., T.S., and X.S. analyzed data; T.K., T.N., H.S., M. Hirose, and M.Y. interpreted results of experiments; T.K. and H.S. prepared figures; T.K., T.N., H.S., and M.Y. drafted manuscript; T.K., T.N., H.S., M.H.-H., S.G., T.S., X.S., M. Hirose, M. Hongo, and M.Y. approved final version of manuscript; M.Y. edited and revised manuscript.

REFERENCES

- Adamson PB, Hull SS Jr, Vanoli E, De Ferrari GM, Wisler P, Foreman RD, Watanabe AM, Schwartz PJ. Pertussis toxin-induced ADP ribosylation of inhibitor G proteins alters vagal control of heart rate in vivo. *Am J Physiol Heart Circ Physiol* 265: H734–H740, 1993.
- Bers DM (editor). Heart failure. In: *Excitation-Contraction Coupling and Cardiac Contractile Force* (2nd ed.). Dordrecht, The Netherlands: Springer, 2008, p. 316–323.
- Binanay C, Califf RM, Hasselblad V, O'Connor CM, Shah MR, Sopko G, Stevenson LW, Francis GS, Leier CV, Miller LW. Evaluation study of congestive heart failure and pulmonary artery catheterization effectiveness: the ESCAPE trial. *JAMA* 294: 1625–1633, 2005.
- Boknik P, Fockenbrock M, Herzig S, Knapp J, Linck B, Luss H, Muller FU, Muller T, Schmitz W, Schroder F, Neumann J. Protein phosphatase activity is increased in a rat model of long-term β -adrenergic stimulation. *Naunyn-Schmiedeberg's Arch Pharmacol* 362: 222–231, 2000.
- Daaka Y, Luttrell LM, Lefkowitz RJ. Switching of the coupling of the β_2 -adrenergic receptor to different G proteins by protein kinase A. *Nature* 390: 88–91, 1997.
- Davare MA, Horne MC, Hell JW. Protein phosphatase 2A is associated with class C L-type calcium channels (Cav1.2) and antagonizes channel phosphorylation by cAMP-dependent protein kinase. *J Biol Chem* 275: 39710–39717, 2000.
- Davies SP, Reddy H, Caivano M, Cohen P. Specificity and mechanism of action of some commonly used protein kinase inhibitors. *Biochem J* 351: 95–105, 2000.
- duBell WH, Rogers TB. Protein phosphatase 1 and an opposing protein kinase regulate steady-state L-type Ca²⁺ current in mouse cardiac myocytes. *J Physiol* 556: 79–93, 2004.
- El-Armouche A, Zolk O, Rau T, Eschenhagen T. Inhibitory G-proteins and their role in desensitization of the adenylyl cyclase pathway in heart failure. *Cardiovasc Res* 60: 478–487, 2003.
- Fabiato A. Calcium-induced release of calcium from the cardiac sarcoplasmic reticulum. *Am J Physiol Cell Physiol* 245: C1–C14, 1983.
- Franzini-Armstrong C, Protasi F. Ryanodine receptors of striated muscles: a complex channel capable of multiple interactions. *Physiol Rev* 77: 699–729, 1997.
- Funakoshi H, Zacharia LC, Tang Z, Zhang J, Lee LL, Good JC, Herrmann DE, Higuchi Y, Koch WJ, Jackson EK, Chan TO, Feldman AM. A₁ adenosine receptor upregulation accompanies decreasing myocardial adenosine levels in mice with left ventricular dysfunction. *Circulation* 115: 2307–2315, 2007.
- Grimm M, Gsell S, Mittmann C, Nose M, Scholz H, Weil J, Eschenhagen T. Inactivation of (G_i α) proteins increases arrhythmogenic effects of β -adrenergic stimulation in the heart. *J Mol Cell Cardiol* 30: 1917–1928, 1998.
- Hackenthal E, Aktories K, Jakobs KH. Pertussis toxin attenuates angiotensin II-induced vasoconstriction and inhibition of renin release. *Mol Cell Endocrinol* 42: 113–117, 1985.
- Hall DD, Feekes JA, Arachchige Don AS, Shi M, Hamid J, Chen L, Strack S, Zamponi GW, Horne MC, Hell JW. Binding of protein phosphatase 2A to the L-type calcium channel Cav1.2 next to Ser¹⁹²⁸, its main PKA site, is critical for Ser¹⁹²⁸ dephosphorylation. *Biochemistry* 45: 3448–3459, 2006.
- Herzig S, Meier A, Pfeiffer M, Neumann J. Stimulation of protein phosphatases as a mechanism of the muscarinic-receptor-mediated inhibition of cardiac L-type Ca²⁺ channels. *Pflügers Arch* 429: 531–538, 1995.
- Herzig S, Neumann J. Effects of serine/threonine protein phosphatases on ion channels in excitable membranes. *Physiol Rev* 80: 173–210, 2000.
- Hess P, Lansman JB, Tsien RW. Different modes of Ca channel gating behaviour favoured by dihydropyridine Ca agonists and antagonists. *Nature* 311: 538–544, 1984.
- Horiuchi-Hirose M, Kashiwara T, Nakada T, Kurebayashi N, Shimojo H, Shibasaki T, Sheng X, Yano S, Hirose M, Hongo M, Sakurai T, Morizumi T, Ueda H, Yamada M. Decrease in the density of t-tubular L-type Ca²⁺ channel currents in failing ventricular myocytes. *Am J Physiol Heart Circ Physiol* 300: H978–H988, 2011.
- Huang B, Wang S, Qin D, Boutjdir M, El-Sherif N. Diminished basal phosphorylation level of phospholamban in the postinfarction remodeled rat ventricle: role of β -adrenergic pathway, G_i protein, phosphodiesterase, and phosphatases. *Circ Res* 85: 848–855, 1999.
- Kawai M, Hussain M, Orchard CH. Excitation-contraction coupling in rat ventricular myocytes after formamide-induced detubulation. *Am J Physiol Heart Circ Physiol* 277: H603–H609, 1999.
- Ke Y, Wang L, Pyle WG, de Tombe PP, Solaro RJ. Intracellular localization and functional effects of P21-activated kinase-1 (Pak1) in cardiac myocytes. *Circ Res* 94: 194–200, 2004.
- Le Guludec D, Cohen-Solal A, Delforge J, Delahaye N, Syrota A, Merlet P. Increased myocardial muscarinic receptor density in idiopathic dilated cardiomyopathy: an in vivo PET study. *Circulation* 96: 3416–3422, 1997.
- Liskova S, Kunes J, Zicha J. Nifedipine-sensitive vascular reactivity of femoral arteries in WKY: the effects of pertussis toxin pretreatment and endothelium removal. *Physiol Res* 56: 663–666, 2007.
- Liu Q, Hofmann PA. Modulation of protein phosphatase 2a by adenosine A₁ receptors in cardiomyocytes: role for p38 MAPK. *Am J Physiol Heart Circ Physiol* 285: H97–H103, 2003.
- Liu R, Ramani B, Soto D, De Arcangelis V, Xiang Y. Agonist dose-dependent phosphorylation by protein kinase A and G protein-coupled receptor kinase regulates β_2 adrenoceptor coupling to G_i proteins in cardiomyocytes. *J Biol Chem* 284: 32279–32287, 2009.
- McDonald TF, Pelzer S, Trautwein W, Pelzer DJ. Regulation and modulation of calcium channels in cardiac, skeletal, and smooth muscle cells. *Physiol Rev* 74: 365–507, 1994.
- Neumann J, Eschenhagen T, Jones LR, Linck B, Schmitz W, Scholz H, Zimmermann N. Increased expression of cardiac phosphatases in patients with end-stage heart failure. *J Mol Cell Cardiol* 29: 265–272, 1997.
- Neumann J, Schmitz W, Scholz H, von Meyerinck L, Doring V, Kalmar P. Increase in myocardial G_i-proteins in heart failure. *Lancet* 2: 936–937, 1988.

30. Shacklock PS, Wier WG, Balke CW. Local Ca²⁺ transients (Ca²⁺ sparks) originate at transverse tubules in rat heart cells. *J Physiol* 487: 601–608, 1995.
31. Sigmund M, Jakob H, Becker H, Hanrath P, Schumacher C, Eschenhagen T, Schmitz W, Scholz H, Steinfath M. Effects of metoprolol on myocardial beta-adrenoceptors and G_{iα}-proteins in patients with congestive heart failure. *Eur J Clin Pharmacol* 51: 127–132, 1996.
32. Sunahara RK, Dessauer CW, Gilman AG. Complexity and diversity of mammalian adenylyl cyclases. *Annu Rev Pharmacol Toxicol* 36: 461–480, 1996.
33. Vatner DE, Sato N, Galper JB, Vatner SF. Physiological and biochemical evidence for coordinate increases in muscarinic receptors and Gi during pacing-induced heart failure. *Circulation* 94: 102–107, 1996.
34. Walsh AH, Cheng A, Honkanen RE. Fostriecin, an antitumor antibiotic with inhibitory activity against serine/threonine protein phosphatases types 1 (PP1) and 2A (PP2A), is highly selective for PP2A. *FEBS Lett* 416: 230–234, 1997.
35. Xiao RP, Cheng H, Lederer WJ, Suzuki T, Lakatta EG. Dual regulation of Ca²⁺/calmodulin-dependent kinase II activity by membrane voltage and by calcium influx. *Proc Natl Acad Sci USA* 91: 9659–9663, 1994.
36. Xu H, Ginsburg KS, Hall DD, Zimmermann M, Stein IS, Zhang M, Tandan S, Hill JA, Horne MC, Bers D, Hell JW. Targeting of protein phosphatases PP2A and PP2B to the C-terminus of the L-type calcium channel Cav1.2. *Biochemistry* 49: 10298–10307, 2010.
37. Yamada M, Ohta K, Niwa A, Tsujino N, Nakada T, Hirose M. Contribution of L-type Ca²⁺ channels to early afterdepolarizations induced by I_{Kr} and I_{Ks} channel suppression in guinea pig ventricular myocytes. *J Membr Biol* 222: 151–166, 2008.
38. Zhu M, Gach AA, Liu G, Xu X, Lim CC, Zhang JX, Mao L, Chuprun K, Koch WJ, Liao R, Koren G, Blaxall BC, Mende U. Enhanced calcium cycling and contractile function in transgenic hearts expressing constitutively active G_{α_s}* protein. *Am J Physiol Heart Circ Physiol* 294: H1335–H1347, 2008.





Contents lists available at SciVerse ScienceDirect

European Journal of Pharmacology

journal homepage: www.elsevier.com/locate/ejphar

Molecular and Cellular Pharmacology

Two mechanistically distinct effects of dihydropyridine nifedipine on Ca_v1.2 L-type Ca²⁺ channels revealed by Timothy syndrome mutationXiaona Sheng^{a,b,c}, Tsutomu Nakada^a, Motohiro Kobayashi^d, Toshihide Kashihara^a, Toshihide Shibazaki^{a,e}, Miwa Horiuchi-Hirose^a, Simmon Gomi^{a,f}, Masamichi Hirose^g, Toshifumi Aoyama^b, Mitsuhiko Yamada^{a,*}^a Department of Molecular Pharmacology, Shinshu University School of Medicine, Matsumoto, Nagano, Japan^b Department of Metabolic Regulation, Institute on Aging and Adaptation, Shinshu University Graduate School of Medicine, Matsumoto, Nagano, Japan^c Department of Neurology, The Second Hospital of Hebei Medical University, Shijiazhuang, Hebei, China^d Department of Molecular Pathology, Shinshu University Graduate School of Medicine, Matsumoto, Nagano, Japan^e Discovery Research Laboratory II, R&D, Kissei Pharmaceutical Co., Ltd., Azumino, Nagano, Japan^f Department of Cardiovascular Medicine, Shinshu University School of Medicine, Matsumoto, Nagano, Japan^g Department of Molecular and Cellular Pharmacology, School of Pharmaceutical Sciences, Iwate Medical University, Morioka, Iwate, Japan

ARTICLE INFO

Article history:

Received 15 January 2012

Received in revised form 10 April 2012

Accepted 12 April 2012

Available online xxx

Keywords:

Ca_v1.2 L-type Ca²⁺ channel

Voltage-dependent inactivation

Dihydropyridine

Nifedipine

Timothy syndrome

Allosteric model

ABSTRACT

Dihydropyridine Ca²⁺ channel antagonists (DHPs) block Ca_v1.2 L-type Ca²⁺ channels (LTCCs) by stabilizing their voltage-dependent inactivation (VDI); however, it is still not clear how DHPs allosterically interact with the kinetically distinct (fast and slow) VDI. Thus, we analyzed the effect of a prototypical DHP, nifedipine on LTCCs with or without the Timothy syndrome mutation that resides in the I–II linker (L_{I–II}) of Ca_v1.2 subunits and impairs VDI. Whole-cell Ba²⁺ currents mediated by rabbit Ca_v1.2 with or without the Timothy mutation (G436R) (analogous to the human G406R mutation) were analyzed in the presence and absence of nifedipine. In the absence of nifedipine, the mutation significantly impaired fast closed- and open-state VDI (CSI and OSI) at –40 and 0 mV, respectively, but did not affect channels' kinetics at –100 mV. Nifedipine equipotentially blocked these channels at –80 mV. In wild-type LTCCs, nifedipine promoted fast CSI and OSI at –40 and 0 mV and promoted or stabilized slow CSI at –40 and –100 mV, respectively. In LTCCs with the mutation, nifedipine resumed the impaired fast CSI and OSI at –40 and 0 mV, respectively, and had the same effect on slow CSI as in wild-type LTCCs. Therefore, nifedipine has two mechanistically distinct effects on LTCCs: the promotion of fast CSI/OSI caused by L_{I–II} at potentials positive to the sub-threshold potential and the promotion or stabilization of slow CSI caused by different mechanisms at potentials negative to the sub-threshold potential.

© 2012 Elsevier B.V. All rights reserved.

1. Introduction

L-type Ca²⁺ channels (LTCCs) mediate Ca²⁺ influx into cells in response to membrane depolarization (Catterall, 2000). The amino acid sequence of their main Ca_v1 subunits is organized into four repeated domains (I–IV), each of which contains six transmembrane segments (S1–S6). Upon membrane depolarization, LTCCs open and are then inactivated. The inactivation of LTCCs is driven by intracellular Ca²⁺ and the membrane potential (VDI) (Hering et al., 2000; Soldatov, 2003; Stotz et al., 2004; Zuhlke et al., 1999). VDI occurs regardless whether channels are open (open-state inactivation (OSI)) or closed (closed-state inactivation (CSI)). Both CSI and OSI of LTCCs occur in a biexponential time course, indicating that LTCCs have at least two kinetically distinct (fast and slow) VDI states. The intracellular linker

between the I and II domains of Ca_v subunits (L_{I–II}) participates in the fast OSI of neuronal P/Q and R-types of Ca²⁺ channels (Herlitze et al., 1997; Stotz et al., 2000, 2004). On the other hand, the mechanism of slow OSI probably includes a more global conformational change of Ca_v subunits (Hering et al., 2000; Kobrinsky et al., 2004; Shi and Soldatov, 2002; Soldatov, 2003) and the immobilization of a gating charge (Hadley and Lederer, 1991; Shirokov et al., 1992).

LTCCs are selectively inhibited by dihydropyridine (DHP) antagonists (Hockerman et al., 1997), which block LTCCs by binding to IIIIS5, IIIIS6 and IVS6 of Ca_v1 subunits and stabilize the nonconducting state of LTCCs with a single Ca²⁺ ion in the selectivity filter (Peterson and Catterall, 2006). DHP antagonists bind to LTCCs with the highest affinity for the inactivated state (Bean, 1984; Lee and Tsien, 1983; Sanguinetti and Kass, 1984). DHP antagonists cause a tonic block and gating charge immobilization of LTCCs at potentials negative to the threshold potential for channel opening (Bean, 1984; Hadley and Lederer, 1991; Lee and Tsien, 1983; Sanguinetti and Kass, 1984). Some DHP antagonists also cause a phasic block of LTCCs by accelerating OSI at potentials positive to the threshold potential (Berjukow and Hering, 2001; Berjukow et

* Corresponding author at: Department of Molecular Pharmacology, Shinshu University School of Medicine, 3-1-1 Asahi, Matsumoto, Nagano 390–8621, Japan. Tel.: +81 263 37 2605; fax: +81 263 37 3085.

E-mail address: myamada@shinshu-u.ac.jp (M. Yamada).

al., 2000; Handrock et al., 1999; Hess et al., 1984; Lacinova et al., 2000; Lee and Tsien, 1983; Sanguinetti and Kass, 1984): however, it has not been clarified how these distinct effects of DHPs take place in relation to the fast and slow CSI/OSI.

Here, we analyzed the effect of a prototypical DHP antagonist nifedipine on the fast and slow CSI/OSI of recombinant rabbit $Ca_v1.2$ LTCCs with or without the G436R mutation that impairs OSI (Raybaud et al., 2006; Yarotsky et al., 2009). This mutation corresponds to the G406R mutation that resides at L_{1-II} in human $Ca_v1.2$ subunits and causes Timothy syndrome, a human disorder associated with fatal ventricular arrhythmias, syndactyly, immune deficiency and autism (Splawski et al., 2004). In this study, we show that nifedipine promotes fast CSI and OSI caused by L_{1-II} at potentials positive to the sub-threshold potential, and promotes or stabilizes slow CSI at potentials negative to the sub-threshold potential.

2. Materials and methods

2.1. Molecular biology

The investigation conformed to the *Guide for the Care and Use of Laboratory Animals* published by the US National Institutes of Health (NIH Publication No. 85-23, revised 1996). This study was approved by the Committee for Animal Experimentation of Shinshu University (approval number: 220024). All experiments described in this study were carried out in accordance with the Guidelines for Animal Experimentation of Shinshu University. Rats were sacrificed by sodium pentobarbital (30 mg/kg) anesthesia administered intraperitoneally, and the heart and brain were excised from the animals. Total RNA of these tissues was extracted with Isogen (Nippon Gene Co. Ltd., Tokyo, Japan) according to the manufacturer's instructions. Total RNA was reverse transcribed by the SuperScript III First-Strand Synthesis System for reverse transcription-PCR (Invitrogen Inc., Carlsbad, CA). The cDNAs of $\alpha_2\delta_1$ (GenBank ID: NM001110847) and β_{2a} (GenBank ID: NM053851) were amplified by PCR with DNA polymerase PrimeSTAR HS from the heart and brain total cDNA, respectively (Takara Bio Inc., Shiga, Japan). The sequence of primers used was 5'-TGATCTTCGATCGCGAAGATGG-3' ($\alpha_2\delta_1$, sense), 5'-AGGGCATGGAATTAAGTTGCAGA-3' ($\alpha_2\delta_1$, antisense), 5'-AGTGTGATTGCCCATGAC-3' (β_{2a} , sense) and 5'-GGCCAATTTCTGTGGTACTT-3' (β_{2a} , antisense). The amplified cDNA fragments encoding $\alpha_2\delta_1$ and β_{2a} were subcloned into pcDNA3.1(-) (Invitrogen) and pcDNA3.1(+)/Hygro (Invitrogen), respectively. The cDNA encoding rabbit $Ca_v1.2$ subunits (GenBank ID: X15539) was generously provided by Prof. William Catterall (University of Washington). The cDNA of $Ca_v1.2$ containing the G436R mutation was generated by the megaprimer method (Kammann et al., 1989). Briefly, the 1st PCR was performed with a primer pair (5'-GAAGATGATCCTTCCCCTGTGCTC-3' and 5'-TCTTTGGAAAACCTCTGCTCAACACACCG-3') and wild-type $Ca_v1.2$ cDNA as a template. The 2nd PCR was performed with the 1st PCR product (mega-primer) and an antisense primer (5'-AAGGATTGACAGTCCCTTGTGCTCAGGTAGTC-3'). Then, a region of wild-type $Ca_v1.2$ cDNA between *Bam*HI and *Afl*III sites was substituted with the PCR product containing the G436R mutation. The nucleotide sequences of all of the constructs were verified with ABI 3130 (Applied Biosystems, Inc., Foster City, CA).

2.2. Cell culture

HEK293 cells (ATCC, Manassas, VA) were maintained in Dulbecco's Modified Eagle's Medium (DMEM) (Invitrogen) containing GlutaMAX (Invitrogen), 10% fetal bovine serum (FBS), 100 U/mL penicillin and 100 μ g/mL streptomycin. HEK293 cells were transfected with pcDNA3.1(-) harboring the $\alpha_2\delta_1$ cDNA with TransFectin Lipid Reagent (Bio-Rad Laboratories, Inc., Richmond, CA) and selected with 800 μ g/mL G418. Among several G418-resistant clones, one clone was chosen based on the expression level of $\alpha_2\delta_1$ protein as assessed by Western blotting. The selected line was further transfected with pcDNA3.1(+)

Hygro harboring the β_{2a} cDNA and selected with 200 μ g/mL hygromycin. Among several hygromycin-resistant clones, one clone was chosen based on the expression level of $\alpha_2\delta_1$ and β_{2a} subunits as assessed by Western blotting (Supplementary Fig. 1). For electrophysiological analysis, cDNAs encoding $Ca_v1.2$ (WT) or $Ca_v1.2$ (G436R) (2 μ g) and that of EGFP (0.4 μ g) were transiently cotransfected into this stable cell line in 2 mL DMEM with TransFectin Lipid Reagent. The expressed LTCC currents were measured 24–72 h after transfection.

2.3. Electrophysiology

The current of LTCCs expressed in HEK293 cells was studied in the whole-cell configuration of the patch clamp technique at 35–37 °C with a patch-clamp amplifier (Axopatch 200B; Molecular Devices Corp., Sunnyvale, CA, or EPC 8; HEKA Instruments Inc., Bellmore, NY). Patch pipettes were fabricated from borosilicate glass capillaries (Kimax-51; Kimble Glass Inc., Vineland, NJ). Capacitative currents were eliminated, and the series resistance was compensated by 75% with the patch-clamp amplifiers. The mean series resistance and cell membrane capacitance were 6.26 ± 0.31 M Ω and 39.80 ± 5.12 pF, respectively. The mean voltage error caused by series resistance was 1.74 ± 0.23 mV at 0 mV. To measure LTCC currents, a gigaohm seal was formed with EGFP-positive cells >80% of which expressed LTCC currents. The external solution was modified Tyrode solution containing (in mmol/L): NaCl, 136.5; KCl, 5.4, CaCl₂, 1.8; MgCl₂, 0.53; HEPES, 5.5; and glucose, 5.5 (pH = 7.4 with NaOH). The pipette solution contained (in mmol/L): D-glutamate, 90; N-methyl-D(-)-glucamine (NMDG), 10; MgCl₂, 5; tetraethylammonium chloride, 20, EGTA, 10; HEPES, 20; and MgATP 3 (pH = 7.3 with CsOH). After the whole-cell configuration had been established, triple pulses to -100, -40 and +10 mV (300 ms duration for each pulse) were continuously applied to the cells from the holding potential of -80 mV every 3 s. Then, the bathing solution was switched to external solution 1 containing (in mmol/L): NMDG, 150, CsCl, 5.4; BaCl₂, 10; MgCl₂, 1.2; 4-aminopyridine, 2; and HEPES, 5 (pH = 7.4 with HCl). About 1 min after currents other than LTCC currents had been suppressed and the amplitude and kinetics of LTCC currents were stable, the membrane potential was held at -80 mV for at least 1 min. The mean peak current amplitude of LTCC channels with or without the G436R mutation (LTCC (G436R) and LTCC (WT)) at 0 mV was -1.55 ± 0.28 and -0.88 ± 0.29 nA, respectively.

To assess the current-voltage relationship of LTCCs, the membrane potential was stepped from -80 mV to potentials between -60 and +60 mV for 500 ms with a 10 mV increment every 60 s. LTCC currents were isolated as the current inhibited by Cd²⁺ (100 μ mol/L) plus nifedipine (10 μ mol/L) (Yamada et al., 2008). Nifedipine was dissolved at 10 mM in DMSO. The final $\leq 0.1\%$ DMSO did not affect LTCC currents. The peak density of LTCC currents evoked by the test pulse was plotted against the membrane potential and fit with the following equation:

$$D_{\text{peak}} = G_{\text{max}} / (1 + \exp((E_{0.5\text{Act}} - E_m) / k_{\text{Act}})) (E_m - E_{\text{rev}}) \quad (1)$$

where D_{peak} is the peak current density; G_{max} , maximum conductance density; $E_{0.5\text{Act}}$, half-maximum activation potential; E_m , membrane potential; k_{Act} , slope factor of activation; and E_{rev} , apparent reversal potential of LTCC currents.

To assess the concentration-dependent effect of nifedipine, the membrane potential was depolarized from the holding potential of -80 mV to 0 mV for 50 ms every 60 s, and nifedipine dissolved in external solution 1 was applied to the cells. The peak LTCC current amplitude in the presence of nifedipine was normalized to that in the presence of 0.1% DMSO, plotted against the concentration of nifedipine and fit with the following equation:

$$I = 1 / (1 + ([NIF] / K_{0.5})^n) \quad (2)$$

where I is normalized peak LTCC current amplitude at 0 mV; $[NIF]$,

concentration of nifedipine; $K_{0.5}$, the half-maximum inhibitory concentration of nifedipine; and n , Hill coefficient.

To analyze the CSI of LTCCs, the membrane potential was depolarized from -80 mV to 0 mV for 20 ms (P1), repolarized to -80 mV for 5 ms, depolarized to -40 mV for varying durations, repolarized to -80 mV for 5 ms and then depolarized to 0 mV for 20 ms (P2) every 120 s. The peak LTCC current amplitude in P2 was normalized to that in P1, plotted against the duration at -40 mV and fit with the following equation:

$$I = A_0 + A_f \exp(-t/\tau_f) + A_s \exp(-t/\tau_s) \quad (3)$$

where I is normalized LTCC current amplitude; A_0 , amplitude of a non-inactivating component; A_f , amplitude of a fast component; t , time after depolarization to -40 mV; τ_f , time constant of a fast component; A_s , amplitude of a slow component; and τ_s , time constant of a slow component.

To analyze the OSI of LTCCs, the membrane potential was depolarized from -80 mV to 0 mV for 20 s every 120 s. The decay of LTCC currents at 0 mV was fit with Eq. (3).

To assess the recovery from inactivation, the membrane potential was stepped from the holding potential of -100 mV to 0 mV for 20 s (P1), to -100 mV for varying durations and then to 0 mV for 20 ms (P2) every 120 s. The peak amplitude of LTCC currents in P2 was normalized to that in P1, plotted against the duration between P1 and P2 and fit with the following equation:

$$r = 1 - A_f \exp(-t/\tau_f) - A_s \exp(-t/\tau_s) \quad (4)$$

where r is recovery; and t , duration at -100 mV. Figs. 3–5 and Table 1 show A_f , A_s , and A_0 values normalized to the sum of these values.

To analyze isochronal inactivation, the membrane potential was depolarized from -80 mV to 0 mV for 50 ms (P1), repolarized to -80 mV for 5 ms, changed to potentials between -100 and 0 mV for 30 s with a 10 mV increment, repolarized to -80 mV for 5 ms, and then depolarized to 0 mV for 50 ms (P2) every 120 s. The peak LTCC current amplitude in P2 was normalized that in P1, plotted against membrane potentials and fit with the following equation:

$$f = 1 / (1 + \exp((E_m - E_{0.5_Inact}) / k_{Inact})) \quad (5)$$

where f is availability; $E_{0.5_Inact}$, half-maximum inactivation potential; and k_{Inact} , slope factor of inactivation.

Recorded membrane currents were low-pass filtered at 10 kHz (-3 dB), digitized at 47.2 kHz with a PCM converter system (VR-10B; Instrutech Corp., New York, NY) and recorded on videocassette tapes. For off-line analysis, data were reproduced, low-pass filtered at 2 kHz (-3 dB), digitized at 5 kHz with an AD converter (ITC16I; Instrutech Corp.) and analyzed with Patch Analyst Pro (MT Corp., Hyogo, Japan).

2.4. Statistical analysis

Data are shown as the means \pm S.E.M. Statistical significance was evaluated with Student's paired or unpaired t -test. For the multiple comparisons of data, analysis of variance with Bonferroni's test was used. $P < 0.05$ was considered significant.

Table 1
Kinetic parameters of L-type Ca^{2+} channels.

| | Wild-type | | | | G436R | | | |
|-----------------------------------|----------------------|----|---------------------------------|----|-----------------------------------|----|----------------------------------|----|
| | Control | n | Nifedipine | n | Control | n | Nifedipine | n |
| Activation | | | | | | | | |
| G_{\max} (pS/pF) | 734 \pm 248 | 7 | | | 569 \pm 139 | 7 | | |
| $E_{0.5_Act}$ (mV) | -10.5 \pm 2.7 | 7 | | | -11.1 \pm 1.6 | 7 | | |
| k_{Act} (mV) | 4.5 \pm 0.5 | 7 | | | 3.5 \pm 0.4 | 7 | | |
| E_{rev} (mV) | 56.7 \pm 1.7 | 7 | | | 53.3 \pm 0.6 | 7 | | |
| Inactivation at 0 mV | | | | | | | | |
| τ_f (s) | 480.78 \pm 62.35 | 21 | 261.20 \pm 44.83 ^a | 13 | 764.94 \pm 125.20 ^d | 9 | 828.73 \pm 171.16 ^d | 11 |
| τ_s (s) | 3121.74 \pm 268.33 | 21 | 2480.40 \pm 313.05 | 13 | 4485.96 \pm 627.43 ^d | 9 | 3256.74 \pm 511.02 | 11 |
| A_f | 0.64 \pm 0.03 | 21 | 0.64 \pm 0.03 | 13 | 0.31 \pm 0.03 ^f | 9 | 0.51 \pm 0.06 ^a | 11 |
| A_s | 0.33 \pm 0.02 | 21 | 0.34 \pm 0.03 | 13 | 0.66 \pm 0.03 ^f | 9 | 0.46 \pm 0.06 ^a | 11 |
| A_0 | 0.03 \pm 0.01 | 21 | 0.03 \pm 0.01 | 13 | 0.03 \pm 0.01 | 9 | 0.04 \pm 0.00 | 11 |
| Inactivation at -40 mV | | | | | | | | |
| τ_f (s) | 0.30 \pm 0.07 | 6 | 0.30 \pm 0.12 | 6 | 0.25 \pm 0.07 | 5 | 0.34 \pm 0.12 | 4 |
| τ_s (s) | 46.50 \pm 11.80 | 6 | 17.84 \pm 3.20 ^a | 6 | 78.46 \pm 24.18 | 5 | 7.66 \pm 2.914 ^a | 4 |
| A_f | 0.21 \pm 0.02 | 6 | 0.36 \pm 0.03 ^b | 6 | 0.11 \pm 0.02 ^c | 5 | 0.27 \pm 0.07 ^a | 4 |
| A_s | 0.37 \pm 0.08 | 6 | 0.35 \pm 0.07 | 6 | 0.40 \pm 0.05 | 5 | 0.38 \pm 0.04 | 4 |
| A_0 | 0.42 \pm 0.08 | 6 | 0.29 \pm 0.07 | 6 | 0.49 \pm 0.04 | 5 | 0.34 \pm 0.07 | 4 |
| Recovery from inactivation | | | | | | | | |
| τ_f (s) | 4.21 \pm 1.07 | 7 | 2.37 \pm 0.43 | 7 | 3.53 \pm 0.42 | 6 | 4.36 \pm 0.70 | 8 |
| τ_s (s) | 42.32 \pm 9.49 | 7 | 77.90 \pm 9.31 ^a | 7 | 55.72 \pm 5.67 | 6 | 78.79 \pm 8.06 ^a | 8 |
| A_f | 0.54 \pm 0.10 | 7 | 0.43 \pm 0.05 | 7 | 0.19 \pm 0.06 ^d | 6 | 0.53 \pm 0.05 ^c | 8 |
| A_s | 0.49 \pm 0.08 | 7 | 0.50 \pm 0.02 | 7 | 0.78 \pm 0.06 ^d | 6 | 0.46 \pm 0.04 ^c | 8 |
| Steady-state inactivation | | | | | | | | |
| $E_{0.5_Inact}$ (mV) | -33.00 \pm 1.84 | 29 | -40.40 \pm 1.83 ^b | 18 | -29.00 \pm 1.19 | 26 | -40.80 \pm 1.32 ^c | 10 |
| k_{Inact} (mV) | 9.01 \pm 0.73 | 29 | 10.50 \pm 1.46 | 18 | 8.38 \pm 0.55 | 26 | 11.60 \pm 0.89 | 10 |

G_{\max} : maximum conductance density; $E_{0.5_Act}$: half-maximum activation potential; k_{Act} : slope factor of activation; E_{rev} : apparent reversal potential; τ_f : time constant for a fast component; τ_s : time constant for a slow component; A_f : relative amplitude of a fast component; A_s : relative amplitude of a slow component; A_0 : relative amplitude of a non-inactivating component; $E_{0.5_Inact}$: half-maximum inactivation potential; k_{Inact} : slope factor of inactivation. ^a: $P < 0.05$ vs. Control; ^b: $P < 0.01$ vs. Control; ^c: $P < 0.001$ vs. Control; ^d: $P < 0.05$ vs. WT; ^e: $P < 0.01$ vs. WT; ^f: $P < 0.001$ vs. WT.

3. Results

3.1. Current–voltage relationship of LTCC (WT) and LTCC (G436R) channels

First, the current–voltage relationship of LTCCs with and without the Timothy mutation (LTCC (G436R) and LTCC (WT), respectively) was analyzed with Ba^{2+} as a charge carrier. As shown in Fig. 1A, both peak LTCC (WT) and LTCC (G436R) currents progressively increased at potentials between -40 and 0 mV and then decreased at potentials between $+10$ and $+50$ mV, yielding almost identical, prototypical U-shaped peak current–voltage relationships (Fig. 1B). Lines are the fit of the averaged data with Eq. (1) with parameters summarized in Table 1. Each parameter was not significantly different between these channels. The decay of the currents reflects OSI. Although the OSI of LTCC (WT) channels was slow, LTCC (G436R) channels exhibited even slower OSI, especially at potentials more positive to 0 mV as previously reported (Barrett and Tsien, 2008; Raybaud et al., 2006; Splawski et al., 2004, 2005; Yarotsky et al., 2009).

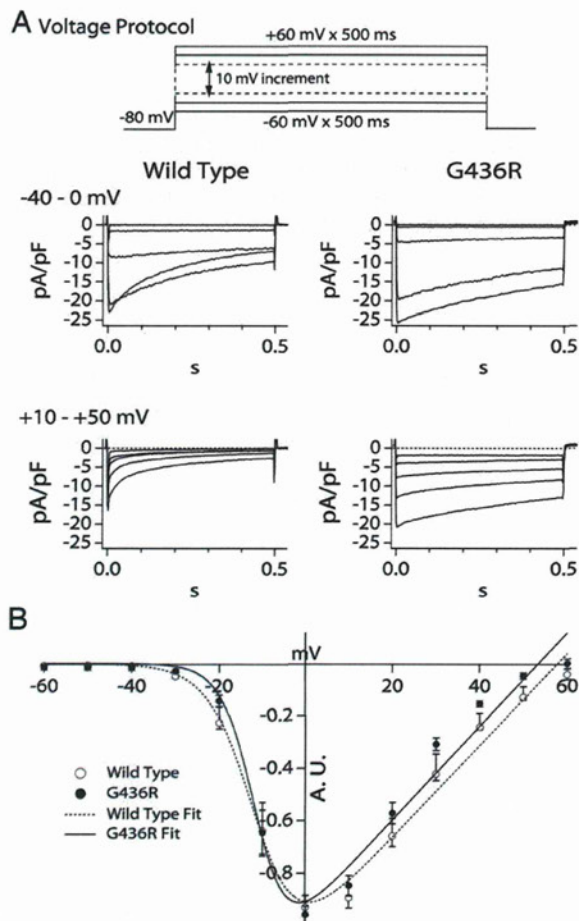


Fig. 1. Current–voltage relationship of L-type Ca^{2+} channels with or without G436R mutation. (A) Top panel: voltage protocol. Middle and bottom panels: representative whole-cell Ba^{2+} currents of wild-type L-type Ca^{2+} channels (LTCC (WT)) and LTCCs with the G436R mutation (LTCC (G436R)) in response to depolarization to potentials between -40 and 0 mV (middle panels) and those between $+10$ and $+50$ mV (bottom panels) with a 10 mV increment. (B) Peak current–voltage relationships of LTCC (WT) and LTCC (G436R) channels. The peak current amplitude in different voltage steps was normalized to the maximum peak current amplitude in each cell. Symbols and bars indicate the mean \pm S.E.M. Lines are the fit of the data with Eq. (1). The parameters obtained with fitting are summarized in Table 1.

3.2. Tonic block of LTCC (WT) and LTCC (G436R) channels by nifedipine at -80 mV

The tonic block of these channels by nifedipine was assessed at the holding potential of -80 mV (Fig. 2). Although LTCC (G436R) exhibited impaired VDI compared with LTCC (WT), nifedipine inhibited both channels in a similar concentration-dependent manner. The fit of the averaged data with Eq. (2) (lines) indicated that the $K_{0.5}$ of nifedipine was 10 and 11 nmol/L for LTCC (WT) and LTCC (G436R) channels, respectively. Thus, nifedipine exerted an almost equipotent tonic block of these channels at -80 mV.

3.3. Effect of nifedipine on LTCC (WT) and LTCC (G436R) channels at -40 mV

We next examined the effect of nifedipine at -40 mV where channels exhibit CSI. In the absence of nifedipine, both LTCC (WT) and LTCC (G436R) channels were inactivated in a time-dependent manner (Fig. 3A). Lines are the fit of the data with a biexponential function (Eq. (3)). Both channels exhibited a similar fast time constant (τ_f), relative amplitude of a slow component (A_s) and relative amplitude of non-inactivating component (A_0) (Fig. 3B, Table 1). A slow time constant (τ_s) tended to be larger in LTCC (G436R) than LTCC (WT) channels, but this difference did not reach statistical significance. The relative amplitude of a fast component (A_f) of LTCC (G436R) channels was significantly smaller than that of LTCC (WT) channels. Nifedipine (3 nmol/L), which inhibited both LTCC (WT) and LTCC (G436R) by $\sim 40\%$ (Fig. 2), significantly increased A_f to a comparable level in these channels. Nifedipine also significantly decreased τ_s in both channels. Consequently, nifedipine diminished the difference in CSI at -40 mV between the channels.

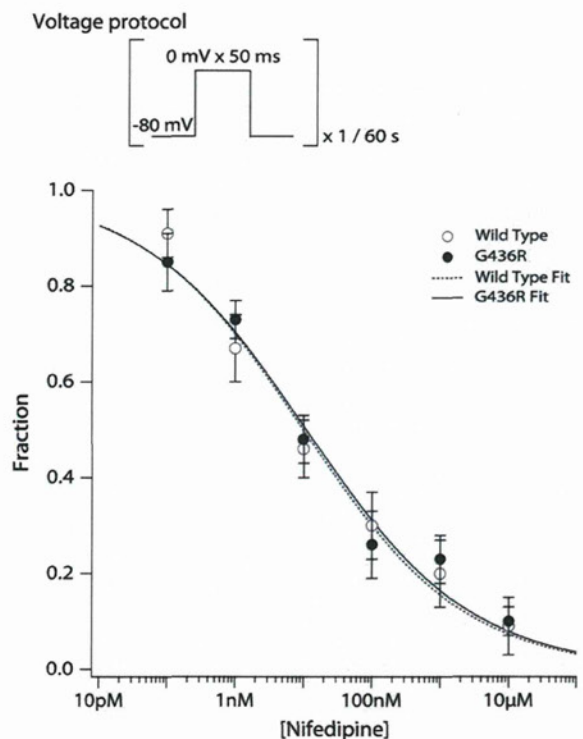


Fig. 2. Concentration-dependent tonic block by nifedipine of LTCC (WT) and LTCC (G436R) channels. Top panel: voltage protocol. Bottom panel: concentration-dependent effect of nifedipine. Nifedipine was cumulatively applied to cells. The peak LTCC current amplitude at 0 mV in the presence of each concentration of nifedipine was normalized to that in the presence of 0.1% DMSO and plotted against the concentration of nifedipine. Symbols and bars indicate the mean \pm S.E.M. Lines are the fit of the data with Eq. (2).

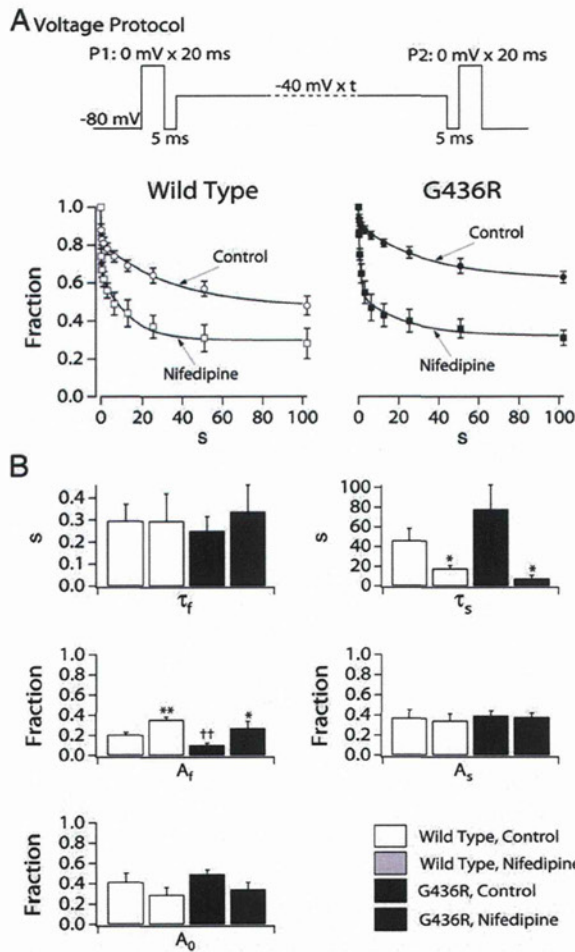


Fig. 3. Effect of nifedipine on inactivation of LTCC (WT) and LTCC (G436R) channels at -40 mV. (A) Top panel: voltage protocol. Bottom panels: a time-dependent decrease in the availability of LTCC (WT) and LTCC (G436R) channels at -40 mV in the absence (CONT) and presence (NIF) of 3 nmol/L nifedipine. Peak LTCC current amplitude in P2 was normalized to that in P1 and plotted against the duration at -40 mV. Symbols and bars indicate the mean \pm S.E.M. Lines are the fit of the data with Eq. (3). (B) Parameters used to fit the decay of availability of LTCC (WT) and LTCC (G436R) channels at -40 mV with Eq. (3) (Table 1). Data are shown as the means \pm S.E.M. *: $P < 0.05$ vs. CONT; **: $P < 0.01$ vs. CONT; †: $P < 0.05$ vs. WT; ††: $P < 0.01$ vs. WT.

3.4. Effect of nifedipine on LTCC (WT) and LTCC (G436R) channels at 0 mV

Fig. 4 shows the effect of nifedipine on LTCC (WT) and LTCC (G436R) currents at 0 mV. To enable both channels to be fully inactivated within a voltage pulse, we applied a 20 s voltage step to cells. In the absence of nifedipine, LTCC (G436R) currents exhibited slower OSI than LTCC (WT) currents (Fig. 4A). The fit of the current decay with a biexponential function (Eq. (3)) indicates that both τ_f and τ_s were significantly larger in LTCC (G436R) than LTCC (WT) channels (Fig. 4B, Table 1). In addition, A_f was significantly smaller and A_s was significantly larger in LTCC (G436R) than LTCC (WT) channels. A_0 was small and not significantly different between the channels. Nifedipine (3 nmol/L) accelerated OSI of both currents. Nifedipine significantly decreased τ_f without affecting other parameters in the LTCC (WT) channels. On the other hand, nifedipine did not significantly affect τ_f or τ_s but significantly increased A_f and decreased A_s in LTCC (G436R) channels. Thus, nifedipine caused a shift of the relative population of the fast and slow components in LTCC (G436R) channels. As a result, the decay of LTCC (G436R) currents in the presence of nifedipine was similar to that of LTCC (WT) currents in the absence of nifedipine.

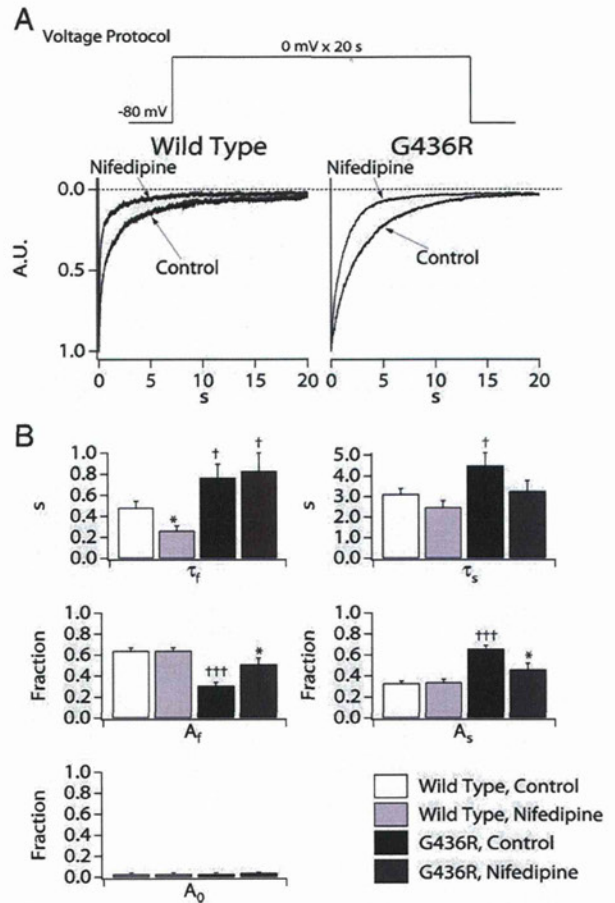


Fig. 4. Effect of nifedipine on inactivation of LTCC (WT) and LTCC (G436R) channels at 0 mV. (A) Top panel: voltage protocol. Bottom panels: representative whole-cell currents of LTCC (WT) and LTCC (G436R) channels at 0 mV in the absence and presence of 3 nmol/L nifedipine. LTCC currents are normalized to the peak current amplitude. (B) Parameters used to fit the decay of whole-cell LTCC (WT) and LTCC (G436R) currents with Eq. (3) (Table 1). Data are shown as the means \pm S.E.M. *: $P < 0.05$ vs. CONT; †: $P < 0.05$ vs. WT; †††: $P < 0.001$ vs. WT.

3.5. Effect of nifedipine on the recovery from inactivation of LTCC (WT) and LTCC (G436R) channels at -100 mV

Fig. 5A shows the time course of the recovery from the OSI of LTCC (WT) and LTCC (G436R) channels at -100 mV in the presence and absence of 3 nmol/L nifedipine. Almost complete OSI was induced by a conditional prepulse to 0 mV for 20 s. Lines are the fit of the averaged data with a biexponential function (Eq. (4)). In the absence of nifedipine, LTCC (G436R) channels recovered from OSI much more slowly than LTCC (WT) channels. Compared with LTCC (WT) channels, LTCC (G436R) channels possessed similar τ_f and τ_s but significantly smaller A_f and larger A_s (Fig. 5B, Table 1). Interestingly, nifedipine decelerated the recovery of LTCC (WT) channels whereas it accelerated that of LTCC (G436R) channels (Fig. 5A). Kinetic analysis indicated that nifedipine significantly increased τ_s but not τ_f in both channels (Fig. 5B, Table 1). Although nifedipine did not affect the other parameters in LTCC (WT) channels, it significantly increased A_f and decreased A_s in LTCC (G436R) channels. As a result, nifedipine diminished the difference in the recovery from VDI between the channels.

3.6. Effect of nifedipine on the isochronal inactivation of LTCC (WT) and LTCC (G436R) channels

We finally examined the effect of nifedipine on the isochronal inactivation of LTCC (WT) and LTCC (G436R) channels in conditional

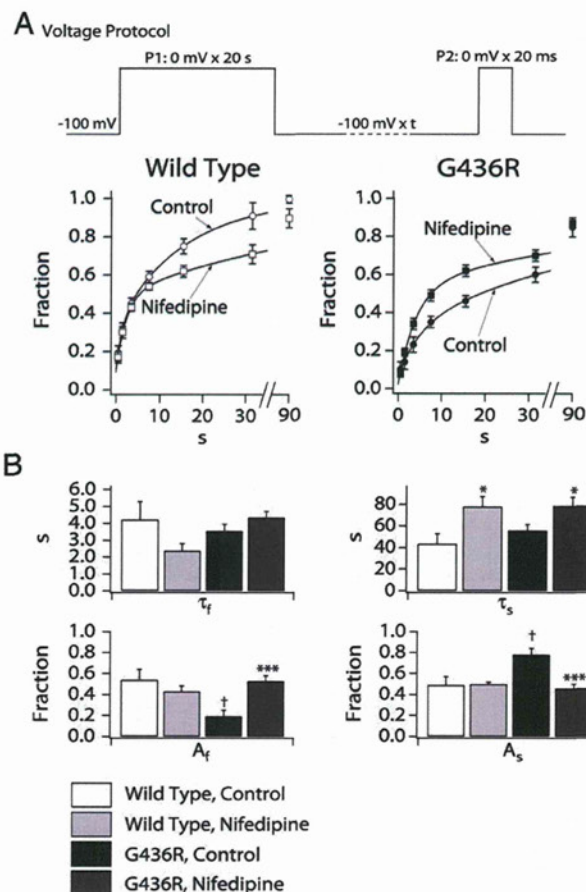


Fig. 5. Effect of nifedipine on recovery of LTCC (WT) and LTCC (G436R) channels at -100 mV. (A) Top panel: voltage protocol. Bottom panels: the recovery from inactivation of LTCC (WT) and LTCC (G436R) channels at -100 mV in the absence and presence of 3 nmol/L nifedipine. Peak amplitude of LTCC currents in P2 was normalized to that in P1, and plotted against the duration between P1 and P2. Symbols and bars indicate the mean \pm S.E.M. Lines are the fit of the data with Eq. (4). (B) Parameters used to fit Eq. (4) to the time course of the recovery from inactivation of LTCC (WT) and LTCC (G436R) channels in the presence and absence of nifedipine (Table 1). Data are shown as the means \pm S.E.M. *; $P < 0.05$ vs. CONT; ***; $P < 0.001$ vs. CONT; †; $P < 0.05$ vs. WT.

pulses to different membrane potentials (Fig. 6). Lines are the fit of the averaged data with a Boltzmann function (Eq. (5)). Neither the half-maximum inactivation potential nor a slope factor was significantly different between LTCC (WT) and LTCC (G436R) channels in the absence of nifedipine (Table 1). Nifedipine significantly caused a leftward shift of the inactivation curve by ~ 7 mV in the LTCC (WT) channels and by ~ 11 mV in the LTCC (G436R) channels.

4. Discussion

4.1. Model of $Ca_v1.2$ L-type Ca^{2+} channels

Both LTCC (WT) and LTCC (G436R) exhibited biexponential CSI (Fig. 3), OSI (Fig. 4) and recovery from OSI (Fig. 5), indicating that they may have fast and slow VDI sates. Fig. 7A illustrates the minimum state diagram of LTCCs. C_0 is a closed state occurring at deeply hyperpolarized potentials whereas C_4 is a pre-open closed state prevailing at the sub-threshold potential (Yarotsky et al., 2009). Upon depolarization from hyperpolarized potentials to supra-threshold potentials, LTCCs transit from C_0 to C_4 and then to an open state (O). Each closed and open state is connected with fast inactivated states (I_{cf0} – I_{cf4} , I_{of}) and slow inactivated states (I_{cs0} – I_{cs4} , I_{os}). Nifedipine independently binds to each state (asterisks).

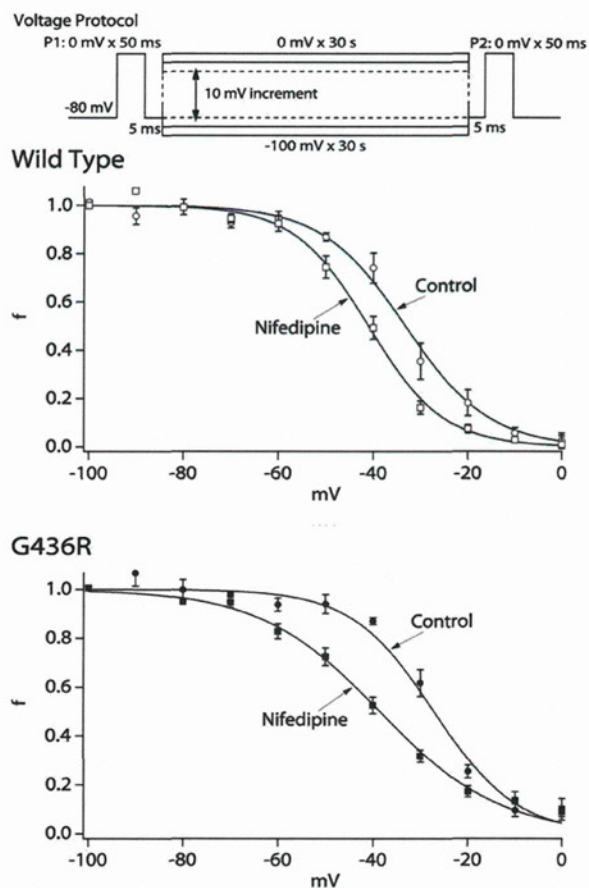


Fig. 6. Effect of nifedipine on isochronal inactivation of LTCC (WT) and LTCC (G436R) channels. Top panel: voltage protocol. Middle and bottom panels: isochronal inactivation of LTCC (WT) and LTCC (G436R) in the absence and presence of 3 nmol/L nifedipine. Peak LTCC current amplitude in P2 was normalized to that in P1 (f) and plotted against membrane potentials. Symbols and bars indicate the mean \pm S.E.M. Lines are the fit of the data with Eq. (5) with parameters summarized in Table 1.

4.2. Comparison of LTCC (WT) and LTCC (G436R) channels in the absence of nifedipine

LTCC (WT) and LTCC (G436R) were activated at potentials positive to -30 mV and exhibited an almost identical current–voltage-relationship (Fig. 1), indicating that activation (C_0 –O) is similar in these channels. It was reported that LTCC (G436R) channels exhibited slower activation and deactivation than LTCC (WT) channels (Yarotsky et al., 2009); however, the steady-state activation does not seem to be significantly different between these channels.

At -40 mV, most LTCCs may transit from C_4 to I_{cf4} and I_{cs4} (Fig. 7A). LTCC (G436R) exhibited smaller A_f than LTCC (WT) (Fig. 3), indicating that the mutation selectively impairs I_{cf4} and thus, that L_{t-II} supports I_{cf4} . Yarotsky et al. (2009) reported that the G436R mutation did not affect CSI at -60 mV. Thus, L_{t-II} seems to support fast CSI at potentials positive to the sub-threshold potential. At 0 mV, LTCCs exhibited OSI (O – I_{of} , O – I_{os}) (Fig. 7A). We found stronger OSI of LTCC (G436R) than previously reported (Fig. 4) (Barrett and Tsien, 2008; Raybaud et al., 2006; Splawski et al., 2004; Yarotsky et al., 2009), probably due to the higher intracellular free Mg^{2+} concentration used in this than previous studies (Brunet et al., 2009). The twice larger A_f than A_s of LTCC (WT) indicates that the O – I_{of} transition predominates over the O – I_{os} transition. Although LTCC (G436R) exhibited significantly larger τ_f and τ_s than LTCC (WT), it showed significantly smaller A_f and larger A_s . Thus, the mutation may more severely impair I_{of} than I_{os} so that I_{os} compensated for the impaired I_{of} . Thus, L_{t-II} may mainly support I_{of} , and the

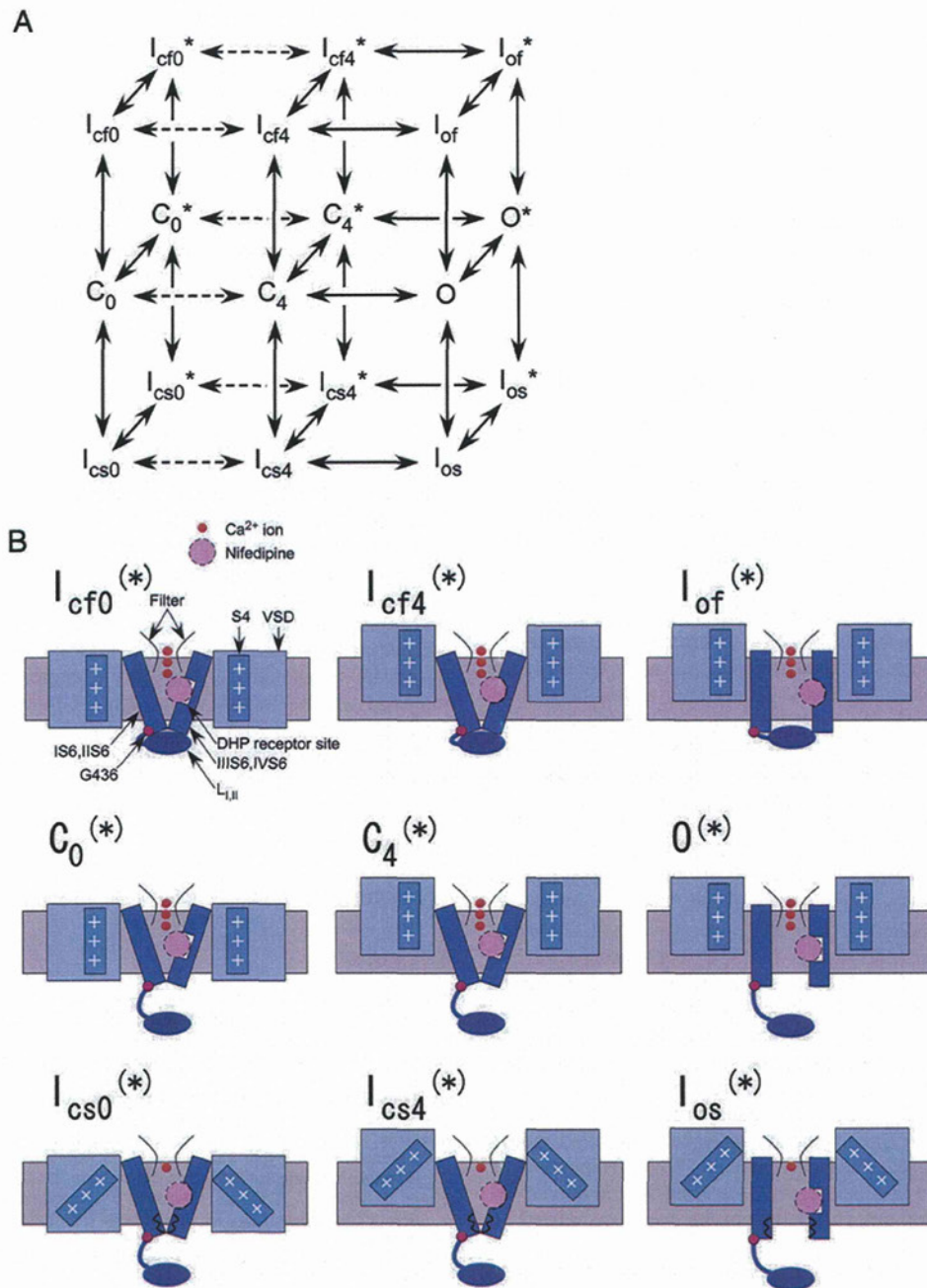


Fig. 7. Allosteric model of L-type Ca²⁺ channels. (A) State diagram of LTCCS. C: closed state; O: open state; I_{cf}: closed fast-inactivated state; I_{cs}: closed slow-inactivated state; I_{of}: open fast-inactivated state; I_{os}: open slow-inactivated state. Asterisks indicate nifedipine-bound states. All interconversions are in principle voltage-dependent. The equilibria and rates for interconversion between nifedipine-free states and between nifedipine-bound states are different. (B) Schematic representation of the side view of LTCCs in the presence and absence of nifedipine. The plasma membrane is depicted as gray squares with the extracellular side upward. Schematics of inner helices formed from I-IVS6, the high-affinity DHP-binding site in III/IVS6, nifedipine, a selectivity filter, Ca²⁺ ions in the selectivity filter, L_{I-II}, G436 and voltage-sensing domains (VSDs) including S4 are shown. The circular DHP-binding site has higher affinity for nifedipine than the square site. Note that the upward movement of VSDs indicates the activation of LTCCs. Fast VDI is shown to be supported by L_{I-II} that occludes the inner mouth of a channel pore by docking to S6. Slow VDI is shown to be associated with gating charge immobilization (indicated by tilted S4), depletion of Ca²⁺ ions in a selectivity filter (indicated by a single Ca²⁺ ion in a filter) and the conformational change of the cytoplasmic part of S6 (indicated by wavy lines). Three Ca²⁺ ions in the selectivity filter indicate conducting states whereas one Ca²⁺ ion in the filter represents non-conducting states.

increased τ_s of LTCC (G436R) may be secondary to the impaired I_{of}. At a voltage step to -100 mV from 0 mV, both channels exhibited biexponential recovery from OSI (Fig. 5), indicating the coexistence of the recovery from I_{of} and I_{os}. Here, we assume that the recovery from I_{of} is faster than that from I_{os} because the recovery was faster after a shorter conditioning pulse in both channels (data not shown). Neither τ_f nor τ_s was significantly different between LTCC (WT) and LTCC

(G436R), indicating the similarity in the kinetics of these channels at -100 mV; however, LTCC (G436R) exhibited significantly smaller A_f and larger A_s than LTCC (WT), which probably reflects the difference in A_f and A_s of OSI in the preceding conditional pulse between the channels (Fig. 3).

Fig. 7B schematically illustrates different states of Ca_v1.2 subunits. Because the G436R mutation mainly impaired fast CSI and OSI, fast

inactivated states are illustrated to arise from the docking of L_{1-II} to S6 (Fig. 7B) (Stotz and Zamponi, 2001; Stotz et al., 2000). Because slow OSI and CSI were not affected by the mutation, they are shown to be caused by other mechanisms such as the conformational change of VSD, depletion of Ca^{2+} ions in the selectivity filter and/or the conformational change of the cytoplasmic end of S6 (Hadley and Lederer, 1991; Peterson and Catterall, 2006; Shi and Soldatov, 2002; Shirokov et al., 1992). Note that nifedipine bound to $Ca_v1.2$ subunits is also depicted and that different shapes of the DHP receptor represent its state-dependent change in the affinity for nifedipine.

4.3. Comparison of the effects of nifedipine on LTCC (WT) and LTCC (G436R) channels

Nifedipine modified the kinetics of LTCC (WT) and LTCC (G436R) upon depolarization (Figs. 3 and 4) and repolarization (Fig. 5). These effects of nifedipine would reflect a voltage-dependent change in the interaction between LTCC and nifedipine. At -40 mV, nifedipine increased A_f in both channels as reported for other DHPs (Berjukow and Hering, 2001; Berjukow et al., 2000) and abolished the difference in A_f between the channels (Fig. 3), indicating that I_{C4} has higher affinity for nifedipine than C_4 (Fig. 7B). It is probable that nifedipine allosterically interacts with L_{1-II} which docks to IIS6 harboring the DHP receptor (Stotz et al., 2000) and thereby augments fast CSI. Nifedipine also decreased τ_s in both channels. It is difficult to interpret this phenomenon if we assume that C_4^* does not become conductive when converted to O^* . If this were the case, CSI would reflect only a time-dependent decrease in C_4 , and nifedipine must accelerate this process. However, the nifedipine-induced $I_{C54}-I_{C54}^*$ transition cannot accelerate the $C_4-I_{C54}-I_{C54}^*$ transition. Thus, we propose that O^* is conductive and that the $C_4-I_{C54}^*$ transition is faster than the C_4-I_{C54} transition (Fig. 7B).

At 0 mV, nifedipine decreased τ_f in LTCC (WT) (Fig. 4). The acceleration of the decay of LTCC Ba^{2+} currents by DHP antagonists arises from the open-channel block (Handrock et al., 1999; Lacinova et al., 2000; Lee and Tsien, 1983; Sanguinetti and Kass, 1984), drug-induced inactivation (Berjukow and Hering, 2001; Berjukow et al., 2000) or acceleration of intrinsic VDI (Hess et al., 1984), but no consensus has been reached. Because we consider that O^* is conducting, we reject the possibility of the open-channel block and propose that the $O^*-I_{O_f}^*$ transition is faster than the $O-I_{O_f}$ transition due to the promoted docking of L_{1-II} to S6. Thus, I_{O_f} may have higher affinity for nifedipine than O (Fig. 7B). On the other hand, nifedipine did not affect τ_s or A_s in LTCC (WT), suggesting that O and I_{O_s} have similar affinity for nifedipine (Fig. 7B). In LTCC (G436R), nifedipine did not significantly affect τ_f or τ_s but significantly increased A_f and decreased A_s . Thus, nifedipine might be unable to accelerate the docking of L_{1-II} carrying the mutation to S6 but still capable of recruiting channels from the over-accumulated I_{O_s} into $I_{O_f}^*$ in LTCC (G436R).

In the recovery at -100 mV, nifedipine did not affect τ_f in either of the channels (Fig. 5), indicating that I_{Cf0} does not have high affinity for nifedipine and thus, is not stabilized by the drug (Fig. 7B). On the other hand, nifedipine significantly increased τ_s in both channels, suggesting that I_{C50} has higher affinity for nifedipine than C_0 (Fig. 7B). Other DHPs also selectively decelerated the slow component of recovery (Berjukow and Hering, 2001; Berjukow et al., 2000; Lacinova et al., 2000; Sanguinetti and Kass, 1984). Similar τ_f and τ_s of LTCC (WT) and LTCC (G436R) indicate that their kinetics were similar at -100 mV also in the presence of nifedipine. Although nifedipine did not affect A_f or A_s in LTCC (WT), it significantly increased A_f and decreased A_s in LTCC (G436R). This may once again reflect the effect of nifedipine on A_f and A_s of OSI in the conditional pulse (Fig. 3). Thus, a kinetic difference between these channels at a deeply hyperpolarized potential is rather minor, which accounts for the insignificant difference in the tonic block of these channels by nifedipine at -80 mV (Fig. 2).

Taken together, nifedipine promoted fast CSI/OSI at potentials positive to the sub-threshold potential whereas it promoted and

stabilized slow CSI at potentials negative to the sub-threshold potential. Hering and his colleagues reported that DHP antagonists (+)- and (-)-isradipine caused an enantioselective tonic block at hyperpolarized potentials but equipotently accelerated the decay of LTCCs at depolarized potentials (Handrock et al., 1999). They found that the former but not the latter effect was disrupted by the mutation of the DHP-binding site in IVS6. Lacinova et al. (2000) showed that the same mutation selectively abolished slow but not fast recovery from VDI in the presence of isradipine. These reports together with the present results suggest that DHP might interact mainly with IIS5/S6 at depolarized potentials, allosterically modulating the docking of L_{1-II} to IIS6 and thereby promoting intrinsic fast VDI. On the other hand, DHP might interact mainly with IVS6 at hyperpolarized potentials and allosterically modulate slow VDI.

5. Conclusion

Nifedipine has two mechanistically distinct effects on LTCCs: the promotion of fast CSI/OSI caused by L_{1-II} at potentials positive to the sub-threshold potential and the promotion or stabilization of slow CSI at potentials negative to the sub-threshold potential. These two different mechanisms may underlie the phasic and tonic block of LTCCs by DHP, respectively.

Nifedipine normalized VDI kinetics of LTCCs with the Timothy syndrome mutation. Yarotsky et al. (2009) also reported that roscovitine accelerates OSI of LTCC (G436R). Thus, these agents may effectively ameliorate the complex excitotoxicity of the Timothy mutation and the resultant developmental and physiological abnormalities in patients with Timothy syndrome.

Supplementary data to this article can be found online at doi:10.1016/j.ejphar.2012.04.029.

Acknowledgement

We are grateful to Ms. Reiko Sakai for secretarial assistance.

References

- Barrett, C.F., Tsien, R.W., 2008. The Timothy syndrome mutation differentially affects voltage- and calcium-dependent inactivation of $Ca_v1.2$ L-type calcium channels. *Proc. Natl. Acad. Sci. U. S. A.* 105, 2157–2162.
- Bean, B.P., 1984. Nitrendipine block of cardiac calcium channels: high-affinity binding to the inactivated state. *Proc. Natl. Acad. Sci. U. S. A.* 81, 6388–6392.
- Berjukow, S., Hering, S., 2001. Voltage-dependent acceleration of $Ca(v)1.2$ channel current decay by (+)- and (-)-isradipine. *Br. J. Pharmacol.* 133, 959–966.
- Berjukow, S., Marksteiner, R., Gapp, F., Sinnegger, M.J., Hering, S., 2000. Molecular mechanism of calcium channel block by isradipine. Role of a drug-induced inactivated channel conformation. *J. Biol. Chem.* 275, 22114–22120.
- Brunet, S., Scheuer, T., Catterall, W.A., 2009. Cooperative regulation of $Ca(v)1.2$ channels by intracellular $Mg(2+)$, the proximal C-terminal EF-hand, and the distal C-terminal domain. *J. Gen. Physiol.* 134, 81–94.
- Catterall, W.A., 2000. Structure and regulation of voltage-gated Ca^{2+} channels. *Annu. Rev. Cell Dev. Biol.* 16, 521–555.
- Hadley, R.W., Lederer, W.J., 1991. Properties of L-type calcium channel gating current in isolated guinea pig ventricular myocytes. *J. Gen. Physiol.* 98, 265–285.
- Handrock, R., Rao-Schymanski, R., Klugbauer, N., Hofmann, F., Herzig, S., 1999. Dihydropyridine enantiomers block recombinant L-type Ca^{2+} channels by two different mechanisms. *J. Physiol.* 521 (Pt 1), 31–42.
- Hering, S., Berjukow, S., Sokolov, S., Marksteiner, R., Weiss, R.G., Kraus, R., Timin, E.N., 2000. Molecular determinants of inactivation in voltage-gated Ca^{2+} channels. *J. Physiol.* 528 (Pt 2), 237–249.
- Herlitze, S., Hockerman, G.H., Scheuer, T., Catterall, W.A., 1997. Molecular determinants of inactivation and G protein modulation in the intracellular loop connecting domains I and II of the calcium channel α_1A subunit. *Proc. Natl. Acad. Sci. U. S. A.* 94, 1512–1516.
- Hess, P., Lansman, J.B., Tsien, R.W., 1984. Different modes of Ca channel gating behaviour favoured by dihydropyridine Ca agonists and antagonists. *Nature* 311, 538–544.
- Hockerman, G.H., Peterson, B.Z., Johnson, B.D., Catterall, W.A., 1997. Molecular determinants of drug binding and action on L-type calcium channels. *Annu. Rev. Pharmacol. Toxicol.* 37, 361–396.
- Kammann, M., Laufs, J., Schell, J., Gronenborn, B., 1989. Rapid insertional mutagenesis of DNA by polymerase chain reaction (PCR). *Nucleic Acids Res.* 17, 5404.
- Kobrinisky, E., Kepplinger, K.J., Yu, A., Harry, J.B., Kahr, H., Romanin, C., Abernethy, D.R., Soldatov, N.M., 2004. Voltage-gated rearrangements associated with differential

- beta-subunit modulation of the L-type Ca(2+) channel inactivation. *Biophys. J.* 87, 844–857.
- Lacinova, L., Klugbauer, N., Hofmann, F., 2000. State- and isoform-dependent interaction of isradipine with the alpha1C L-type calcium channel. *Pflügers Arch.* 440, 50–60.
- Lee, K.S., Tsien, R.W., 1983. Mechanism of calcium channel blockade by verapamil, D600, diltiazem and nitrendipine in single dialysed heart cells. *Nature* 302, 790–794.
- Peterson, B.Z., Catterall, W.A., 2006. Allosteric interactions required for high-affinity binding of dihydropyridine antagonists to Ca(V)1.1 Channels are modulated by calcium in the pore. *Mol. Pharmacol.* 70, 667–675.
- Raybaud, A., Dodier, Y., Bissonnette, P., Simoes, M., Bichet, D.G., Sauve, R., Parent, L., 2006. The role of the GX9GX3G motif in the gating of high voltage-activated Ca2+ channels. *J. Biol. Chem.* 281, 39424–39436.
- Sanguinetti, M.C., Kass, R.S., 1984. Voltage-dependent block of calcium channel current in the calf cardiac Purkinje fiber by dihydropyridine calcium channel antagonists. *Circ. Res.* 55, 336–348.
- Shi, C., Soldatov, N.M., 2002. Molecular determinants of voltage-dependent slow inactivation of the Ca2+ channel. *J. Biol. Chem.* 277, 6813–6821.
- Shirokov, R., Levis, R., Shirokova, N., Rios, E., 1992. Two classes of gating current from L-type Ca channels in guinea pig ventricular myocytes. *J. Gen. Physiol.* 99, 863–895.
- Soldatov, N.M., 2003. Ca2+ channel moving tail: link between Ca2+-induced inactivation and Ca2+ signal transduction. *Trends Pharmacol. Sci.* 24, 167–171.
- Splawski, I., Timothy, K.W., Sharpe, L.M., Decher, N., Kumar, P., Bloise, R., Napolitano, C., Schwartz, P.J., Joseph, R.M., Condouris, K., Tager-Flusberg, H., Priori, S.G., Sanguinetti, M.C., Keating, M.T., 2004. Ca(V)1.2 calcium channel dysfunction causes a multisystem disorder including arrhythmia and autism. *Cell* 119, 19–31.
- Splawski, I., Timothy, K.W., Decher, N., Kumar, P., Sachse, F.B., Beggs, A.H., Sanguinetti, M.C., Keating, M.T., 2005. Severe arrhythmia disorder caused by cardiac L-type calcium channel mutations. *Proc. Natl. Acad. Sci. U. S. A.* 102, 8089–8096 (discussion 8086–8088).
- Stotz, S.C., Zamponi, G.W., 2001. Structural determinants of fast inactivation of high voltage-activated Ca(2+) channels. *Trends Neurosci.* 24, 176–181.
- Stotz, S.C., Hamid, J., Spaetgens, R.L., Jarvis, S.E., Zamponi, G.W., 2000. Fast inactivation of voltage-dependent calcium channels. A hinged-lid mechanism? *J. Biol. Chem.* 275, 24575–24582.
- Stotz, S.C., Jarvis, S.E., Zamponi, G.W., 2004. Functional roles of cytoplasmic loops and pore lining transmembrane helices in the voltage-dependent inactivation of HVA calcium channels. *J. Physiol.* 554, 263–273.
- Yamada, M., Ohta, K., Niwa, A., Tsujino, N., Nakada, T., Hirose, M., 2008. Contribution of L-type Ca2+ channels to early afterdepolarizations induced by I Kr and I Ks channel suppression in guinea pig ventricular myocytes. *J. Membr. Biol.* 222, 151–166.
- Yarotsky, V., Gao, G., Peterson, B.Z., Elmslie, K.S., 2009. The Timothy syndrome mutation of cardiac CaV1.2 (L-type) channels: multiple altered gating mechanisms and pharmacological restoration of inactivation. *J. Physiol.* 587, 551–565.
- Zuhlke, R.D., Pitt, G.S., Deisseroth, K., Tsien, R.W., Reuter, H., 1999. Calmodulin supports both inactivation and facilitation of L-type calcium channels. *Nature* 399, 159–162.

